

Mid-infrared spectra of late-type stars: Long-term evolution

J. D. Monnier¹, T. R. Geballe², and W. C. Danchi¹

ABSTRACT

Recent ground-based mid-infrared spectra of 29 late-type stars, most with substantial dust shells, are compared to ground-based spectra of these stars from the 1960s and 1970s and to IRAS-LRS spectra obtained in 1983. The spectra of about half the stars show no detectable changes, implying that their distributions of circumstellar material and associated dust grain properties have changed little over this time interval. However, many of the stars with strong silicate features showed marked changes. In nearly all cases the silicate peak has strengthened with respect to the underlying continuum, although there is one case (VY CMa) in which the silicate feature has almost completely disappeared. This suggests that, in general, an oxygen-rich star experiences long periods of gradual silicate feature strengthening, punctuated by relatively rare periods when the feature weakens. We discuss various mechanisms for producing the changes, favoring the slow evolution of the intrinsic dust properties (i.e., the chemical composition or grain structure). Although most IRAS spectra agree well with ground-based spectra, there are a number of cases where they fall well outside the expected range of uncertainty. In almost all such cases the slopes of the red and blue LRS spectra do not match in their region of overlap.

Subject headings: stars: AGB and post-AGB, stars: circumstellar matter, stars: mass-loss, stars: variables, ISM: dust

1. Introduction

Although the first mid-infrared (5-20 μm) spectra of late-type stars were taken over thirty years ago, no systematic comparison with more recent spectra of identical sources has ever been made. In the late 1960's and early 1970's, Merrill, Stein, and collaborators obtained a homogeneous set of mid-infrared spectra on a large set of oxygen-rich and carbon-rich asymptotic giant branch (AGB) stars. In the 1980's, the Infrared Astronomical Satellite (IRAS) provided an atlas of 8-22 μm spectra, but on the question of comparison with previously observed sources the IRAS Explanatory Supplement merely stated: "The comparison showed satisfactory results (IRAS 1988, pp. IX-20)."

¹Space Sciences Laboratory, University of California, Berkeley, Berkeley, CA 94720-7450

²Gemini Observatory, 670 North A'ohoku Place, University Park, Hilo, HI 96720

Recently, we published mid-infrared spectra of red giants and supergiants, many of which show long-period variability, with increased temporal coverage to resolve spectral changes taking place on a pulsational time scale (Monnier, Geballe & Danchi 1998=MGD98).

MGD98 identified stars that showed significant spectral shape variations during a pulsational cycle and characterized the observed changes. Some observers in the past have interpreted spectral changes as reflecting long-term changes rather than pulsational ones (e.g., Forrest, Gillett & Stein 1975), but their data did not adequately sample a sufficiently long time interval to test this interpretation. Cognizant of these issues, we now compare these three homogeneous sets of data to search for significant long-term changes in spectral shape.

The 8-13 μm spectra of most of these stars contain significant emission from circumstellar dust grains. If this dust is forming in steady state at a typical condensation temperature of $\sim 1200\text{ K}$, then the inner dust radius is at $\sim 3\text{-}4 R_\star$, corresponding to about 10 AU for Mira variables. Most of the mid-infrared dust emission comes from this region containing the hottest dust. If the dust is moving at typical velocities for molecules observed in the outflows ($\sim 10\text{ km s}^{-1}$) then the emitting dust within $\sim 20\text{ AU}$ is replenished every 10 years. Hence, we expect an investigation of mid-infrared spectra over a 25 year time span to effectively probe the temporal uniformity of the mass-loss around a given star.

In this paper we first introduce and describe the data sets used for spectral comparison. Care was taken to understand the particular calibration procedures and most of the spectra were extracted from large homogeneous sets. Also by comparing these sets of data as a whole, systematic biases in any given data set may be discovered through comparison with the other two. Indeed, in our comparison of the data sets we have discovered a subset of miscalibrated LRS spectra in the IRAS database. Lastly, we discuss the implications of our results for the understanding of mass-loss processes on the AGB and single out a few stars for special comment.

2. The Data Sets

This paper makes use entirely of published mid-infrared spectra, and we refer the interested reader to the original articles for complete observing details. For most stars considered here, three epochs of data exist in the literature: one from the late 1960's or early 1970's (Epoch I), one from the IRAS-LRS Atlas observed in 1983 (Epoch II), and, lastly, UKIRT data from the mid-1990's (Epoch III). See Table 1 for additional information on the target stars. We will now describe the data set used for each epoch and the calibration issues unique to each.

Merrill & Stein (1976abc) published the most extensive set of mid-infrared spectra during the late 1960's and 1970's and we have used their data when available. This strategy makes the comparison of spectra taken decades apart less susceptible to varying calibration techniques of the observers. Since all spectra by a given observer may suffer from the same systematic errors, these errors may be identified by comparison with a more recent, homogeneous set of spectra.

In addition, spectra from Gillett, Low & Stein (1968), Hackwell (1972), Forrest, Gillett & Stein (1975), and Giguere, Woolf, & Webber (1976) were used to supplement the 3-epoch data set available for analysis. All these authors calibrated their spectra by observing standard stars and assuming blackbody temperatures (e.g., α CMa as a 10000 K blackbody), although the calibration star used for each particular spectrum was rarely documented. Occasionally α Boo (K1.5III) and α Tau (K5III) were used, being approximated as 4000 K blackbodies (Gillett & Forrest 1973), a problematic assumption due to absorption in the fundamental band of SiO (Cohen & Davies 1995). However, recent work (Cohen, Walker & Witteborn 1992) has found that the spectrum of α Tau can be fit very well by a 3800 K blackbody between 8 and 20 μm , and hence these calibrations made by Merrill, Stein, and others are quite satisfactory in this wavelength regime.

The InfraRed Astronomical Satellite (IRAS) was launched in January 1983 and operated for nearly a year. It was outfitted with the Low-Resolution Spectrometer (LRS) which collected thousands of spectra at wavelengths between 8 and 22 μm . The spectrometer measured two overlapping wavelength ranges: one from 7.7 to 13.4 μm and another from 11.0 to 22.6 μm . The spectral shape was calibrated by assuming the intrinsic α Tau spectrum was equal to a 10000 K blackbody; this and additional information can be found in the IRAS Explanatory Supplement (1988). Cohen, Walker & Witteborn (1992) measured the mid-infrared spectrum of α Tau independently and found systematic deviations from the ideal Planck spectrum, and their correction factors were applied to all IRAS-LRS data before comparison in this paper. The IRAS-LRS Atlas data were obtained from an internet repository maintained by Kevin Volk at the University of Calgary (http://iras3.iras.ucalgary.ca/~volk/getlrs_plot.html) and further description of the data set, including scans not originally included in the IRAS-LRS Atlas, can be found elsewhere (Volk & Cohen 1989; Volk et al. 1991; Kwok, Volk, & Bidelman 1997).

The most recent epoch of mid-infrared spectrophotometry considered here was carried out at the United Kingdom Infra-Red Telescope (UKIRT) from 1994 to 1997 (Monnier, Geballe & Danchi 1998). All standard stars used for flux calibration were of spectral type K0 or earlier, so that absorption in the fundamental band of SiO, which is very prominent in late K and M giants and supergiants, is minimal in the ratioed spectra and does not affect the shapes of the reduced spectra.

In this paper we do not concern ourselves with the absolute flux level of the mid-infrared spectra, because of the difficulty in reconciling the broad-band filter bandpasses used by IRAS and the early workers, which would be required to precisely compare the absolute photometry. In addition, previous workers sampled the stellar spectrum at incongruous pulsational phases. For example, Merrill & Stein (1976ab) presented relative spectrophotometry accompanied by a table of broad-band fluxes; unfortunately, spectra obtained at various and undocumented phases during the pulsational cycle of variable stars were averaged together. This is also true for the IRAS-LRS spectra; the published Atlas spectra result from an averaging of multiple scans taken at different times.

Therefore, we present only relative spectra, normalized to the average broadband 8-13 μm

flux. Only the recent UKIRT data (Monnier, Geballe & Danchi 1998) sampled the stellar spectra throughout the pulsational cycle, and we include spectra nearest to maximum and minimum for all stars when possible. Although adding some clutter to the figures, this allows one to determine if spectral shape differences are likely due to pulsation effects, rather than long-term evolution of the dust shell properties.

Observers during Epochs I and III generally used photometric apertures about $5''$ in size, while IRAS had a larger one ($6' \times 15'$). The Egg Nebula is the only source in this paper whose mid-infrared emission is known to be extended on the former scale. The Infrared Spatial Interferometer has surveyed a number of these bright mid-infrared sources (e.g., Danchi et al. 1994) and showed that nearly all of the mid-infrared emission occurs on scales smaller than $5''$. However, direct imaging of faint emission around these stars has rarely been done. In a few cases, some emission has been detected outside of the small aperture used by Epoch I and III observers. In particular, Sloan and collaborators have detected distant silicate material around α Ori (Sloan et al. 1993) and carbon grains around IRC +10216 (Sloan & Egan 1995). While only contributing a small fraction of the total flux, it is possible that such missing flux can contribute significantly to spectral features in the mid-infrared region in some cases. Hence some small differences observed between Epoch II (IRAS) and the other data sets may be attributable to such an effect.

3. Results

3.1. Categorization Procedure

In order to avoid the ambiguity associated with subjective classifications, a quantitative measure of spectral variability was developed to identify sources exhibiting statistically significant long-term evolution of their mid-infrared spectral shapes. A simple χ^2 -based statistic, defined in the Appendix, allows robust identification of stars exhibiting long-term changes in their spectra. This statistic takes into account the pulsation-related spectral changes observed in MGD98 as well as measurement error in determining the likelihood of long-term spectral variability.

Using the procedure outlined in the Appendix, two relevant statistics, $\chi_{\text{Epoch I}}^2$ and χ_{IRAS}^2 have been calculated for all sources, and these results appear in Table 1. These values are indicative of the spectral changes occurring between Epoch I and Epoch III and between Epoch II (IRAS) and Epoch III, respectively. Epoch I and Epoch II data were not quantitatively compared to each other because the spectra did not temporally sample the pulsational cycle of the sources.

The stars in this survey showed a continuum of variability; some stars evinced virtually no variability, while others showed obvious spectral changes. In order to divide our sample, we have adopted the cutoff value of $\chi^2 = 1.5$ to indicate significant variability. Based on these quantities, the stars have been divided into three categories and presented in Figures 1-3. Figure 1 contains the spectra of 6 stars which are consistent with the hypothesis of no spectral evolution between all

three epochs. Figure 2 contains spectra of 9 stars that show good agreement between Epoch I and Epoch III, but in which the IRAS spectra appear discrepant. Finally, Figure 3 presents 14 stars whose spectral shapes are significantly different between Epoch I and Epoch III, independent of the IRAS data.

3.2. Constant Stars

Figure 1 contains spectra of stars whose spectral shapes have not changed, within known uncertainties, between all three epochs under study. Quantitatively, the selection criterion for inclusion in this figure is $\chi_{\text{Epoch I}}^2 \leq 1.50$ and $\chi_{\text{IRAS}}^2 \leq 1.50$; in addition, three stars with no available Epoch I data are included here. Many of these stars are calibrators because of their general lack of variability and relatively little dust emission (e.g., α Boo, α Tau, δ Oph). The excellent agreement found for these stars provides confidence that changes in spectral shape described in the next two sections are indeed real and not the result of the differing calibration procedures of the individual observers. Note that CIT 3 is highly variable, and the large spectral shape changes occurring during its pulsational cycle would mask all but the most dramatic long-term spectral evolution.

3.3. IRAS data

Figure 2 presents spectra of stars that show excellent agreement between the earliest and the most recent epochs ($\chi_{\text{Epoch I}}^2 \leq 1.5$), but whose IRAS measurements show systematic disagreement ($\chi_{\text{IRAS}}^2 > 1.5$) with recent data. In a few obvious cases, the miscalibration of one of the IRAS-LRS detectors appears responsible (e.g., α Her) for this discrepancy. The red and blue detectors of IRAS-LRS share a common wavelength region between 11.1 and 13.4 μm , and should report self-consistent spectral fluxes. In the Appendix, we define the statistic σ_{overlap} which quantifies how well the observed spectral slopes in the two LRS detectors agree in the overlap region. In short, a straight line is fitted to the ratio of the blue and red data in the overlap region. For self-consistent data, the slope should be zero and σ_{overlap} is the number of standard deviations away from zero of the best-fit slope. Hence, values above 3 are very unlikely ($< 1\%$) to occur by chance for well-calibrated data and Gaussian random noise. This statistic has been calculated for all IRAS data in this paper and the results can be found in Table 1.

The spectra in this figure are ordered by increasing σ_{overlap} ; hence, spectra at the end of the figure show this miscalibration effect most strongly. There is no evidence for miscalibration problems in the overlap region ($\sigma_{\text{overlap}} \lesssim 2.0$) for the first three spectra (SW Vir, RX Boo, Egg Nebula). The large angular size of the Egg Nebula is the most likely explanation for the different spectral shapes observed for that star (see previous discussion at the end of §2). However, RX Boo and SW Vir are not known to be extended, and the apparent spectral variability may indicate the presence of transient strengthening/weakening of the silicate feature around these two Semi-regular

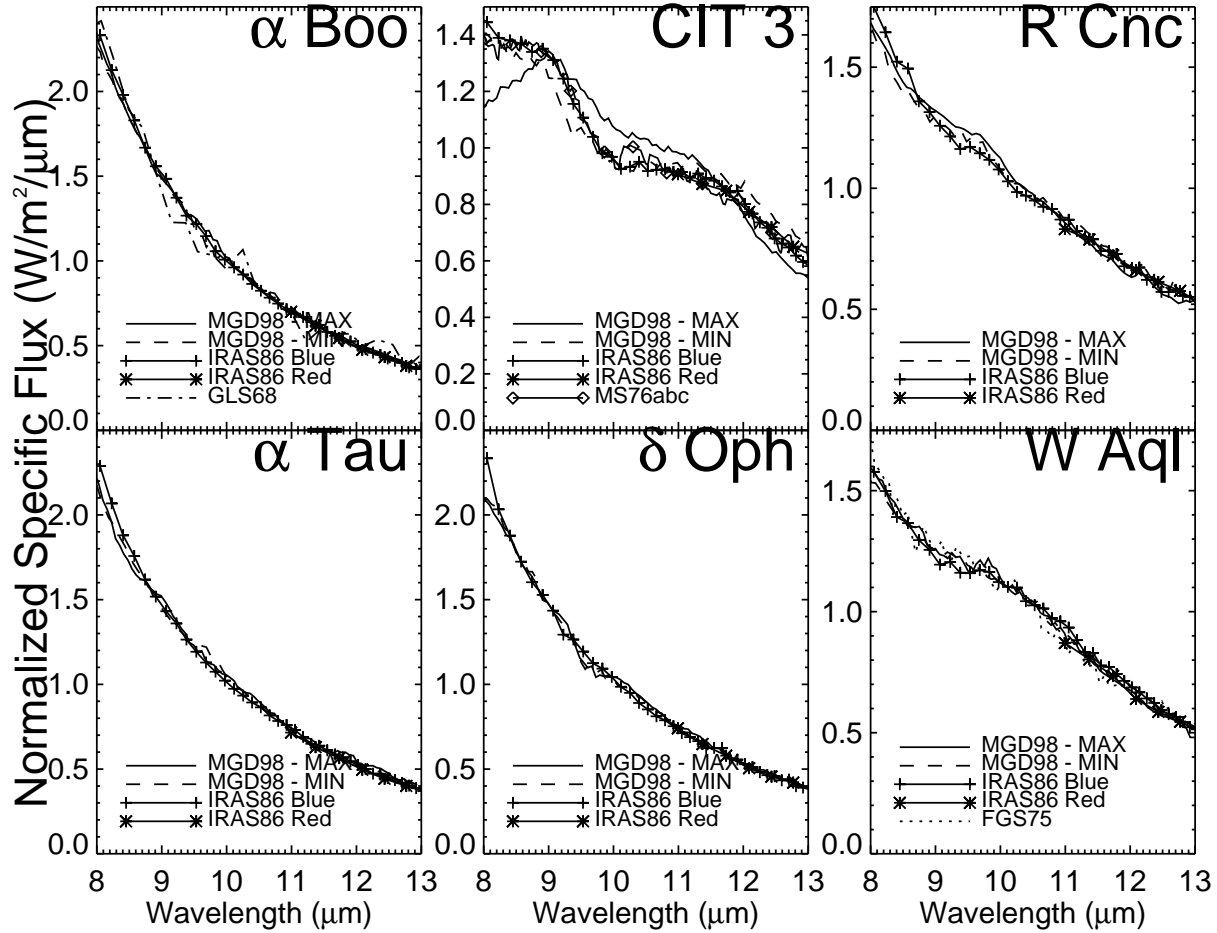


Fig. 1.— Normalized mid-infrared spectra of late-type stars that showed no apparent changes in spectral shape using data from Epochs I, II, and III. Epoch III spectra near maximum and minimum flux are shown. Spectra references are for Gillett, Low, & Stein (1968=GLS68), Hackwell (1972=Hackwell72), Forrest, Gillett, & Stein (1975=FGS75), Merrill & Stein (1976=MS76abc), IRAS Science Team (1986=IRAS86), and Monnier, Geballe, & Danchi (1998=MGD98).

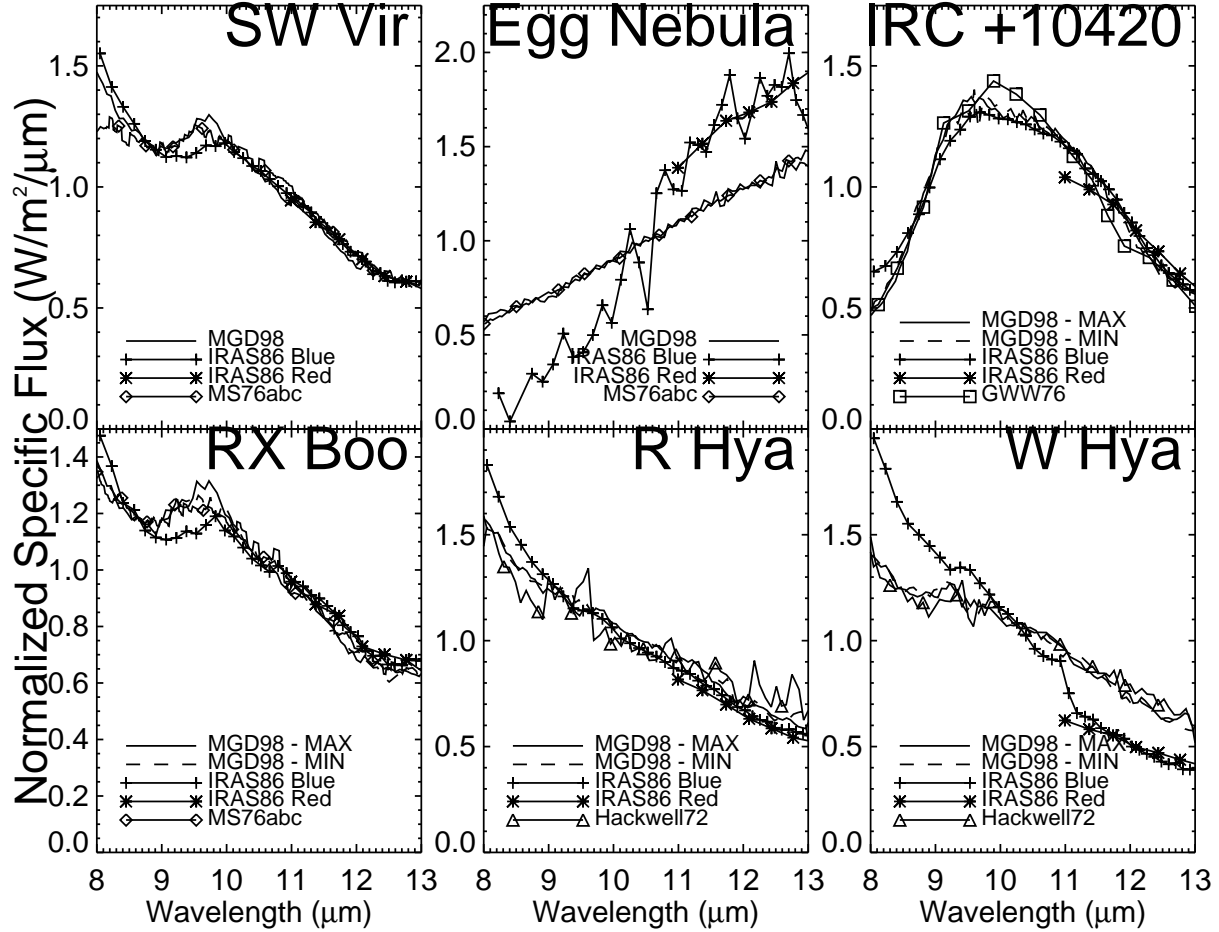


Fig. 2.— Normalized mid-infrared spectra of late-type stars that showed no apparent changes in spectral shape between Epochs I and III, but whose IRAS spectra (Epoch II) appear discrepant. Refer to Figure 1 for spectral references.

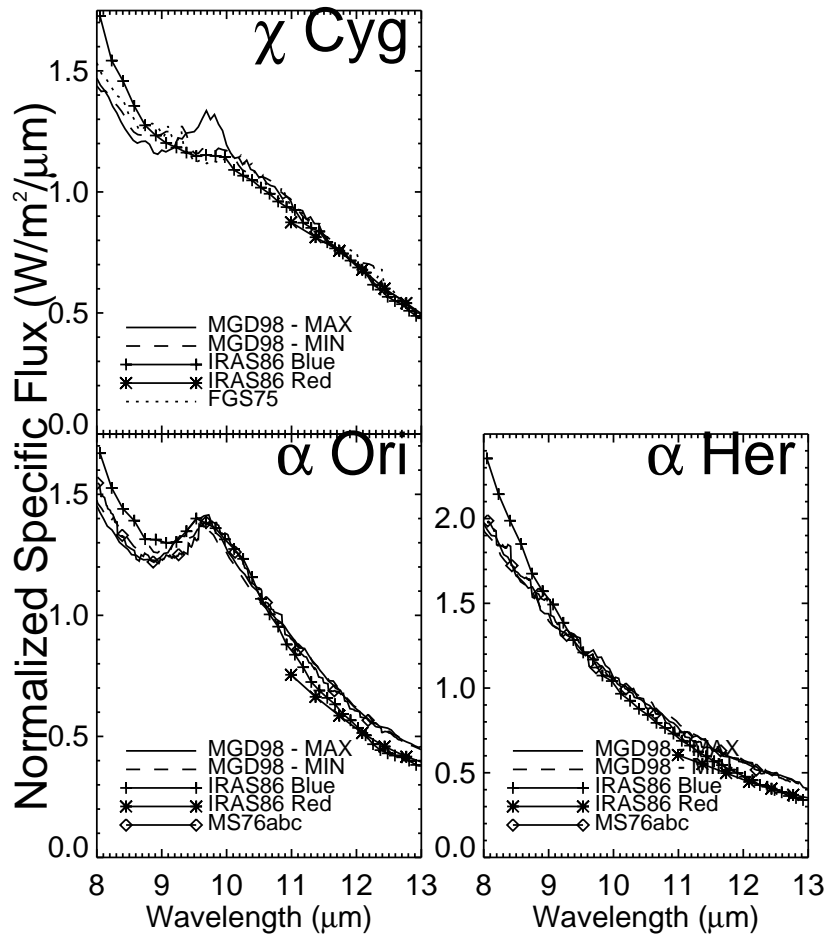


Fig. 2.— continued

variable stars. Note that only one Epoch III spectrum exists for SW Vir, hence the importance of pulsation-related variability on this star’s spectral shape is not known. In fact, the formal $\chi_{\text{Epoch I}}^2$ for SW Vir is larger than 1.5, but was included in this figure because differences between the Epoch I and Epoch III data are likely due to pulsation effects not quantified by the statistic.

By ordering the spectra by σ_{overlap} , we can see a systematic spectral “tilt” associated with the spectral slope-mismatch. All the IRAS spectra in Figure 2 with large σ_{overlap} also evince an overall spectral shape which is *bluer* than the Epoch I and III data, easily seen as excess emission between 8 and 9 μm . Hence, it is reasonable to conclude that most of the IRAS-LRS data with high σ_{overlap} values have some residual miscalibration, not previously identified, and appear slightly bluer than in reality. Inspection of Table 1 reveals that 11 of the 29 IRAS-LRS spectra considered here have $\sigma_{\text{overlap}} \geq 3.0$. An understanding and future correction of this miscalibration may be useful.

3.4. Evidence for long-term changes

The spectra of the remaining 14 stars appear in Figure 3a-c, and all show significant changes between Epochs I and III. The Epoch II spectra of some of these stars are flawed in the same manner as discussed in §3.3, while others appear to be largely consistent with one epoch or the other, or intermediate between the two. All spectra here have $\chi_{\text{Epoch I}}^2 > 1.5$ and the χ_{IRAS}^2 statistic was not used in determining membership in this class. In addition, these 14 stars have been further subdivided based on the type of spectral variability observed.

3.4.1. Strong silicate emission features

Figure 3a contains the spectra of 7 stars whose strong silicate features show long term variability. Because the dust grains around these stars have such strongly wavelength-dependent opacities near 10 μm , the profile of the silicate feature and its equivalent width are highly sensitive to changes in the spectral emission characteristics, temperature, and optical depth structure of the dust shells. Many of these stars were identified in MGD98 as possessing silicate features that change shape even during a pulsational cycle. However, the observed changes between Epoch I and III lie outside the envelope of variation previously observed.

The changes observed in the emission spectra of the dust could be due to long-term variations in the properties of the dust particles themselves. Dust optical constants can be affected by changing chemical abundances or other physical conditions in the stellar atmospheres (see MGD98) as the star evolves, perhaps linked to thermal pulses or other nuclear shell burning phenomena. Changes in the elemental composition may be the only way to explain the dramatic change in the VY CMa spectrum (see below).

Alternatively, these differences may be due to episodic mass-loss events, the observed variations

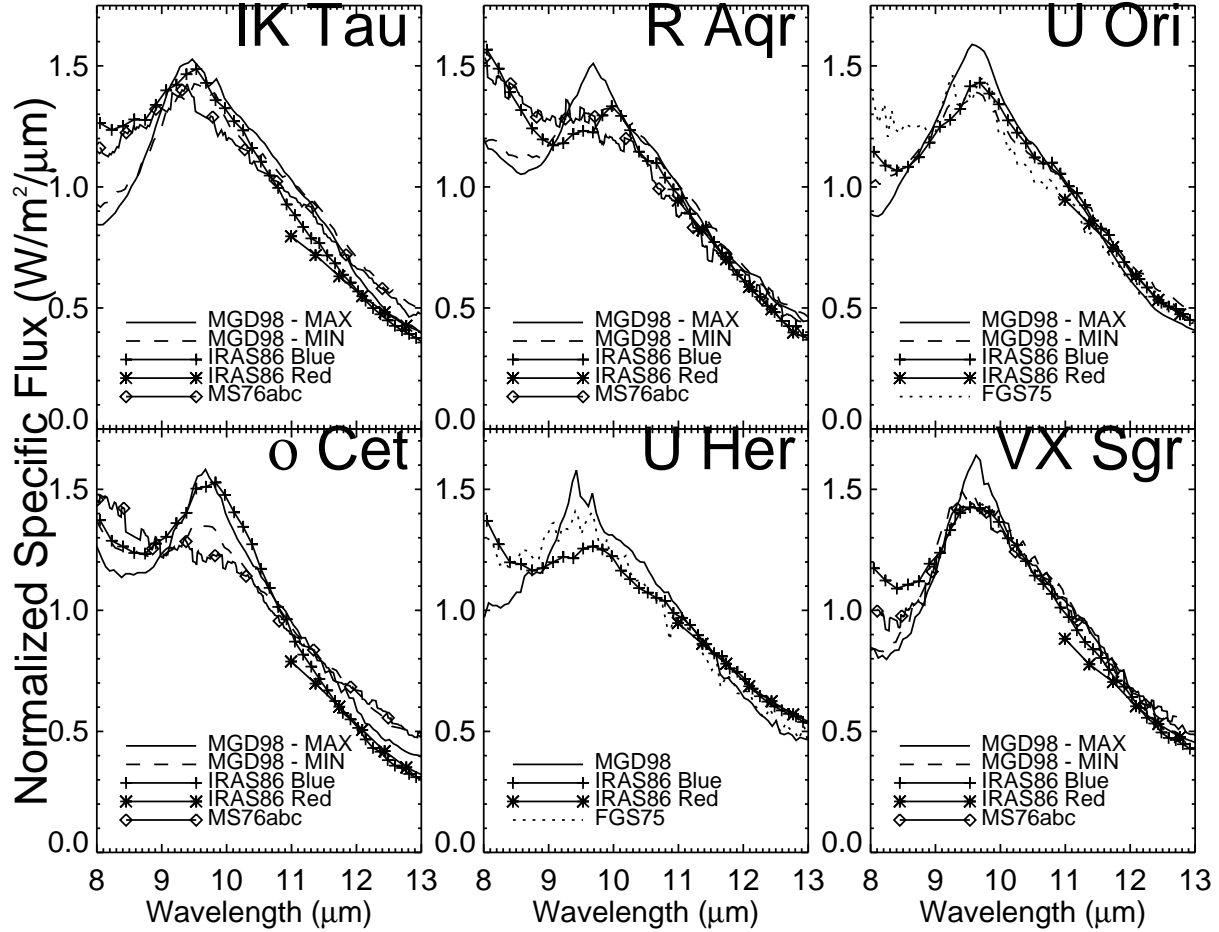


Fig. 3.— Normalized mid-infrared spectra of late-type stars that showed significant changes in spectral shape between Epochs I and III, independent of the IRAS data. Refer to Figure 1 for spectral references. *a*. Stars with strong silicate emission features.

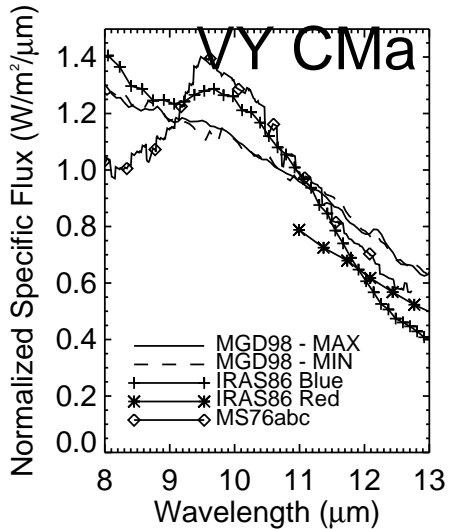


Fig. 3a.— continued

in the spectra being consistent with an overall cooling of the circumstellar dust shell. However, interferometric observations of these dust shells in the infrared indicate the presence of dust close to the expected condensation radius (Dyck et al. 1984; Danchi et al. 1994), making it difficult to understand why the mean dust shell temperatures should all be decreasing in time. See MGD98 for more detailed discussions on the dust temperature’s effect on the mid-infrared spectra. In short, the observed changes in the spectral shape require a large temperature change which would imply a dust-star separation incompatible with interferometer measurements.

Regardless of the mechanism for producing the observed changes, the fact that few stars showed a decrease in the silicate feature peak relative to the continuum suggests that these stars spend most of their time building up their silicate peaks. Assuming the silicate strengthening has been gradual and continuous over the last 25 years, the typical time between episodes of silicate feature weakening must be much longer than that probed here. Considering that 5 Mira variables with the strongest silicate emission features all showed the same systematic change in spectral shape, we estimate that this time scale is greater than about 125 years. Because of the fewer number of supergiant candidates, we can only say the time scale relevant for these stars is likely to be greater than ~ 40 years.

3.4.2. Spectral slope changes

Figure 3b shows the spectra of 4 stars whose Epoch I and Epoch III spectra differ in slope by an amount well outside that expected from the statistical error in the measurements. In all cases here,

the spectra have become redder, consistent with a long-term cooling of the dust shell. However, the slopes of the Epoch II spectra are not always intermediate to the Epoch I and III spectra, and hence the spectral tilt may have different origin (e.g., R Leo). Variation in the dust production on time scale of 10-20 years could produce such changes, and would be in general agreement with conclusions based on interferometry (e.g., Danchi et al. 1994). However, we note that a slight spectral miscalibration across the wavelength band can also mimic this effect.

3.4.3. Excess variability of the carbon stars

The spectra of the 3 carbon stars in our sample are found in Figure 3c. MGD98 noted that the spectra from the carbon stars showed more apparent variability on a pulsation time scale than oxygen-rich stars with weak silicate features. The long-term variability reported here is also fairly small, but statistically significant. Variability of the complex dust distributions recently observed around a few such stars using interferometric techniques (Haniff & Buscher 1998; Weigelt et al. 1998; Tuthill, Monnier, & Danchi 1999) may play a role in this observed enhanced variability.

3.5. Comments on individual sources

α Ori: The silicate feature has shifted toward slightly shorter wavelengths now. While not consistent with a generally cooling of the dust shell, this may be caused by slight replenishing of inner dust shell as recently observed by Bester et al. (1996). Although poor calibration could explain the difference, changes in the optical properties of the dust as it ages may be important here.

Egg Nebula: Observers during Epochs I and III generally used photometric apertures about 5'' in size, while IRAS had a larger one (6' \times 15'). Because this nebula is extended on the same scale as the smaller, ground-based apertures, direct comparison of the data sets is difficult.

IRC +10420: The Epoch I data for this source is rather noisy and was included only to demonstrate that no gross changes in the silicate feature have occurred (see VY CMa comments below). The high noise level prevents a detailed comparison between Epoch I and II data sets.

R Hya: Peculiarly, the IRAS-LRS Atlas spectra from the blue and red detectors agree well in slope but are noticeable offset from one another (see Figure 2).

U Her: Because MGD98 only published a single observation of this source, the identification of this source as experiencing a long-term spectral variation is suspect. However, the Epoch I observation appears visually to be outside the typically envelope of pulsation-related variability seen in the other spectra of Figure 3a. New observations of this source during a pulsational cycle are important to resolve this ambiguity.

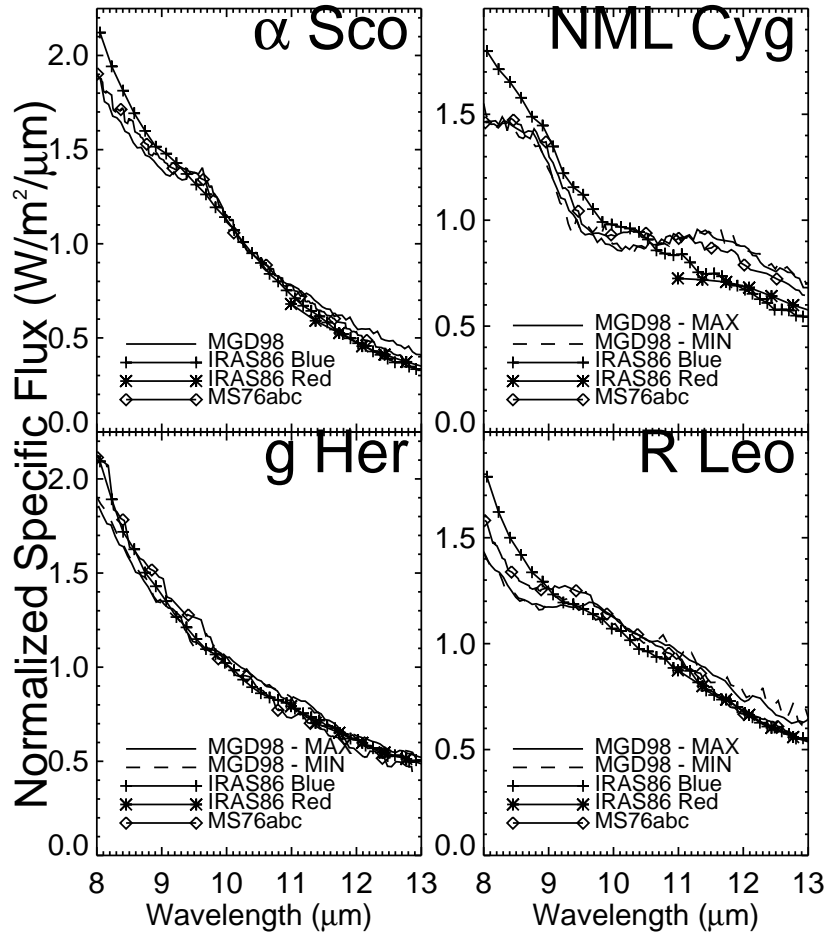


Fig. 3.— *b*. Stars evincing long-term spectral tilts.

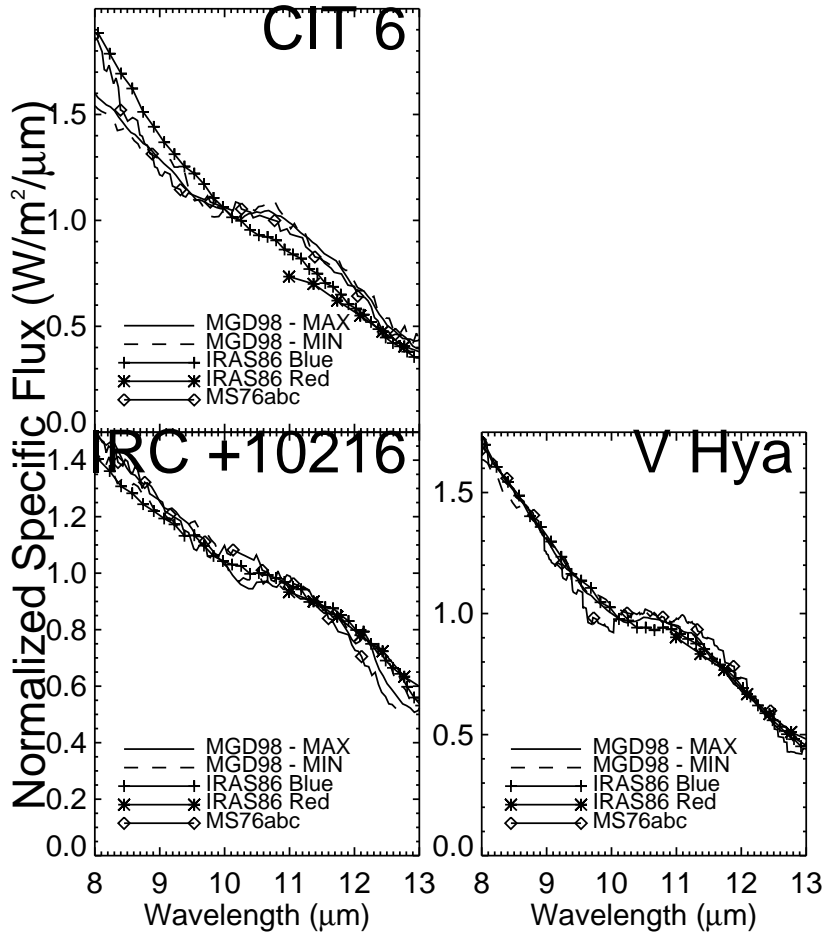


Fig. 3.— *c.* Carbon stars, displaying enhanced variability.

VY CMa: The mid-infrared spectrum of the red supergiant *VY CMa* has undergone a remarkable change over the last 25 years (Monnier, Geballe & Danchi 1998). What was once one of the strongest silicate features observed by Merrill & Stein (1976a) is now nearly flat and featureless. Although the spectral slopes of the IRAS-LRS red and blue detectors are significantly different, it appears that the strength of the feature was intermediate in 1983 to that observed before and after and suggests the spectral change did not occur “overnight,” but instead evolved over a number of years. A significant increase in optical depth, sufficient to cause self-absorption in the silicate feature, could explain most of the flattening of the spectrum. However, a self-absorbed silicate feature usually shows more residual structure (e.g., NML Cyg, CIT 3) than apparent here, implying the emission properties of the dust grains themselves have undergone a relatively rapid transformation. It is not known what physical mechanism could cause such a dramatic change in the dust properties, but perhaps could be due to a change in the chemical abundances. This may

be related to the “remarkable change” in the infrared polarization between 1970 and 1974 observed by Maihara et al. (1976). See Monnier et al. (1999) for recent high-resolution observations which sheds some light on this mystery.

4. Conclusions

We have compiled a multi-epoch set of mid-infrared spectra on 29 stars spanning a ~ 25 year observing period. This comparison has established the high quality of published ground-based spectra and allowed an investigation into the long-term stability of dust shells and their properties.

The mid-infrared spectral shapes of about half of the target stars have remained nearly constant over the entire period of time. This suggests that the mass-loss rates have not changed significantly during the last 25 years. This constancy has allowed us to show that IRAS-LRS spectra may be somewhat miscalibrated when the slopes of the red and blue spectra do not match in their shared wavelength region.

Most of the stars showing strong silicate features have experienced an increase in the strength of the silicate peak relative to the continuum. This is naturally explained if an oxygen-rich star generally experiences long periods of gradual silicate feature strengthening, punctuated by relatively rare periods when the feature weakens. The physical conditions regulating dust formation may be varying on this long time scale, affecting the optical properties of the dust particles in the outflow. Alternatively, general cooling of the dust shells over the last 25 years can explain this effect, although this hypothesis is at odds with interferometric observations of hot dust around many of these stars. The dramatic near-disappearance of the silicate emission feature around VY CMa deserves attention, and may lead to new insights into mass-loss processes around evolved stars.

This rudimentary analysis highlights the not surprising fact that the circumstellar environments of late-type stars are not always simple, and that assumptions of steady-state dust production on time scales of decades can not always be justified. These data provide further evidence that mass-loss characteristics and dust signatures change not only on the time scale of the large amplitude pulsations, but on significantly longer ones as well.

The authors would like to thank Kevin Volk for providing IRAS-LRS spectra via his internet repository and for valuable discussion of its contents. JDM thanks C. D. Matzner and A. P. Zengulys for numerous discussions. This research has made productive use of NASA’s Astrophysics Data System Abstract Service. This analysis was supported by the National Science Foundation (Grants AST-9315485 & AST-9731625) and by the Office of Naval Research (OCNR N00014-89-J-1583 & FDN0014-96-1-0737).

A. Definition of χ^2 and σ_{overlap} statistics

The analysis in the body of this paper has made use of a few simple statistics to evaluate the constancy of stellar spectral shapes between epochs widely separated in time. The purpose of this Appendix is to precisely define the parameters χ^2 and σ_{overlap} used in the text. Since only the spectral *shapes* are under scrutiny here, all comparisons are done between spectra which have been normalized by their mean fluxes.

A.1. Definition of χ^2

The χ^2 statistic is simply a measure of how well a previous spectra *fits* a recent one. The χ^2 defined here deviates from the classical one in two respects. Firstly, we report the reduced χ^2 , i.e. the $\Sigma\chi_i^2$ per degree of freedom, instead of the $\Sigma\chi_i^2$; hence, values greater than unity indicate a poor fit. Secondly, the uncertainty in the recent spectra (MGD98) is a combination of pulsation-related variability and measurement error. A uniform 2.0% relative uncertainty was assumed for all MGD98 data points (as estimated in the original paper). However, if the spectral shapes of MGD98 data at flux maximum and minimum showed greater variation than this due to pulsation-related effects, then the observed variation was used to indicate the spectral shape uncertainty.

If we denote the normalized MGD98 spectra at flux maximum and minimum by S_λ^{max} and S_λ^{min} , then the wavelength-dependent uncertainty, δS_λ , is defined below, where $S_\lambda^{\text{mean}} = \frac{1}{2}[S_\lambda^{\text{max}} + S_\lambda^{\text{min}}]$,

$$\delta S_\lambda = \text{Maximum} \left(\frac{1}{2}[S_\lambda^{\text{max}} - S_\lambda^{\text{min}}], 0.02 \times S_\lambda^{\text{mean}} \right). \quad (\text{A1})$$

Measurement error for the previous epoch data, σ_λ , was estimated from the scatter of data values over small wavelength intervals. These sources of uncertainty were combined in quadrature, and the reduced- χ^2 evaluated as prescribed below. The averaging was done over the wavelength range 8.1 to 12.5 μm , slightly smaller than the fiducial bandpass due to limited coverage of a few Epoch I spectra.

$$\chi_{\text{Epoch I}}^2 = \left\langle \frac{[S_\lambda^{\text{mean}} - S_\lambda^{\text{Epoch I}}]^2}{(\delta S_\lambda)^2 + (\sigma_\lambda^{\text{Epoch I}})^2} \right\rangle_\lambda. \quad (\text{A2})$$

Although the above equation was written for Epoch I, the χ_{IRAS}^2 statistic has the identical form.

A.2. Definition of σ_{overlap}

This statistic was used to identify IRAS-LRS Atlas spectra whose blue and red detector results were inconsistent in their common, overlapping wavelength region, between 11.0 and 13.1 μm . As with the previously defined χ^2 statistic, we chose a very simple statistical criterion.

By restricting ourselves to the overlap region defined above, we can define a wavelength-dependent ratio by dividing the data from the blue detector by the data from the red detector. Self-consistency would demand that this ratio be equal to unity for all values in the wavelength overlap region (within the noise). However, it was apparent from the data (e.g., α Her) that occasionally the blue detector displayed a steeper slope than that observed by the red detector. This effect caused the ratio of the blue to red values to have a slope across the wavelength overlap region. A line was fit (using the least-squares criterion) through the ratio vs. wavelength curve data, and parameter uncertainties were estimated using standard bootstrap-sampling techniques. This produced an estimate of the line slope and its standard deviation. The σ_{overlap} parameter is simply the magnitude of this slope divided by the standard deviation. For perfectly calibrated data and Gaussian noise, more than 99% of the slope determinations should be within 3 standard deviations of 0.0. An identical analysis performed on simulated data indeed confirmed that we statistically expect fewer than 1 of 29 fits to be outside of 3 standard deviations. However, 11 of the 29 spectra (38%) surveyed here were found with σ_{overlap} greater than 3.0 (see Table 1), indicating that spectral slope mismatches in the overlap region do affect a significant fraction of the IRAS data considered.

REFERENCES

- Bester, M., Danchi, W. C., Hale, D., Townes, C. H., Degiacomi, C. G., Mekarnia, D., & Geballe, T. R. 1996, *ApJ*, 463, 336
- Cohen, M., Walker, R. G., & Witteborn, F. C. 1992, *AJ*, 104, 2030
- Cohen, M. & Davies, J. K. 1995, *MNRAS*, 276, 715
- Danchi, W. C., Bester, M., Degiacomi, C. G., Greenhill, L. J., & Townes, C. H. 1994, *AJ*, 107, 1469
- Dyck, H. M., Zuckerman, B., Leinert, Ch., & Beckwith, S. 1984, *ApJ*, 287, 801
- Draine, B. T. & Lee, H. M. 1984, *ApJ*, 285, 89
- Forrest, W. J., Gillett, F. C., & Stein, W. A. 1975, *ApJ*, 195, 423
- Gillett, F. C., & Forrest, W. J. 1973, *ApJ*, 179, 483
- Gillett, F. C., Low, F. J., & Stein, W. A. 1968, *ApJ*, 154, 677
- Giguere, P. T., Woolf, N. J., & Webber, J. C. 1976, *ApJ*, 207, L195
- Hackwell, J. A. 1972, *A&A*, 21, 239
- Haniff, C. A. & Buscher, D. F. 1998, *A&A*, 334, L5
- IRAS Science Team. 1986, *A&AS*, 65, 607
- IRAS Explanatory Supplement, 1988, *IRAS Catalogs and Atlases, Volume 1*, NASA RP-1190 (U.S. Government Printing Office, Washington, D.C.)
- Kwok, S., Volk, K., and Bidelman, W. P. 1997, *ApJS*, 112, 557
- Maihara, T., Noguchi, K., Oishi, M., Okuda, H., & Sato, S. 1976, *Nature*, 259, 465
- Merrill, K. M., & Stein, W. A. 1976a, *PASP*, 88, 285
- Merrill, K. M., & Stein, W. A. 1976b, *PASP*, 88, 294
- Merrill, K. M., & Stein, W. A. 1976c, *PASP*, 88, 874
- Monnier, J. D., Geballe, T. R., & Danchi, W. C. 1998, *ApJ*, 502, 833
- Monnier, J. D., Tuthill, P. G., Lopez, B., Cruzalebes, P., Danchi, W. C., & Haniff, C. A., 1999, *ApJ*, 512
- Sloan, G. C., Grasdalen, G. L., & Levan, Paul D. 1993, *ApJ*, 404, 328

Sloan, G. C. & Egan, M.P. 1995, ApJ, 444, 452

Tuthill, P. G., Monnier, J. D., & Danchi, W. C. 1999, Proc. of IAU Symposium 191, in press

Volk, K. & Cohen, M. 1989, AJ, 98, 931

Volk, K., Kwok, S., Stencel, R. E., & Brugel, E. 1991, ApJS, 77, 607

Weigelt, G., Balega, Y., Bloeker, T., Fleischer, A. J., Osterbart, P., & Winters, J. M. 1998, A&A, 333, L51

Table 1. Stellar Characteristics

Figure Number	Name	Alternate Names	Spectral Type ^a	Variable Type ^a	$\chi^2_{\text{Epoch I}}$	χ^2_{IRAS}	σ_{overlap}	Epoch I Reference
1	α Boo		K1.5III		1.00	0.37	0.01	1
	α Tau		K5III		n/a	0.83	1.43	n/a
	CIT 3	WX Psc IRC+10011	M9	Mira	0.84	1.50	3.35	2
	δ Oph		M0.5III		n/a	0.74	1.12	n/a
	R Cnc		M7IIIe	Mira	n/a	0.91	1.00	n/a
	W Aql		S4.9	Mira	0.61	0.42	2.14	4
	2	SW Vir	IRC+00230	M7III	SRb	2.02	1.52	0.11
RX Boo			M7.5III	SRb	1.28	3.26	0.18	5
Egg Nebula		AFGL 2688	F5Iae		0.81	13.36	0.22	6
R Hya			M7IIIe	Mira	1.34	3.18	0.36	7
IRC+10420		V1302 Aql	F8Ia		0.19	2.00	2.96	3
W Hya			M8e	SRa	0.73	34.87	2.49	7
χ Cyg			S8,K0III	Mira	1.29	1.96	4.43	4
α Ori			M1.5Iab	SRc	1.13	6.94	4.84	5
α Her			M5		1.08	7.23	12.11	5
3a	IK Tau	IRC+10050	M6me	Mira	4.79	7.85	12.70	2
	<i>o</i> Cet	Mira	M7IIIe	Mira	3.09	4.99	2.41	5
	R Aqr		M7IIIpe	Mira	12.35	3.68	0.60	5
	U Her		M7III	Mira	3.76	14.29	2.27	4
	U Ori		M8III	Mira	2.49	0.23	1.11	4
	VX Sgr		M4Iae	SRb	1.61	2.98	8.79	5
	VY CMa		M5Iae	SR	41.31	7.14	7.39	5
	3b	α Sco		M1.5Ib	SRa	2.83	14.25	10.07
g Her			M6III	SRb	7.39	2.86	0.82	5
NML Cyg		IRC+40448	MI ^b	SR	4.80	28.36	3.29	2
R Leo			M8IIIe	Mira	10.11	9.29	0.28	5
3c	CIT 6	RW LMi IRC+30219	C	Mira	3.19	15.11	11.81	2
	IRC+10216	CW Leo	C	Mira	1.71	1.55	1.99	2
	V Hya		C9	SRa	3.53	0.76	5.31	5

^aFrom Simbad Database

^bSupergiant classification based on Morris & Jura (1983)

References. — 1. Gillett, Low & Stein 1968; 2. Merrill & Stein 1976b; 3. Giguere, Woolf & Webber 1976; 4. Forrest, Gillett & Stein 1975; 5. Merrill & Stein 1976a; 6. Merrill & Stein 1976c; 7. Hackwell 1972